SOCIETÀ TOSCANA
DI
Scienze Naturali
RESIDENTE IN PISA

ATTI
DELLA
SOCIETÀ TOSCANA
DI
SCIENZE NATURALI

MEMORIE • SERIE A • VOLUME CXXV • ANNO 2018

Edizioni ETS

Con il contributo del Museo di Storia Naturale dell'Università di Pisa

Fondazione
Cassa di Risparmio
di Lucca

e della Fondazione Cassa di Risparmio di Lucca

INDICE - *CONTENTS*

Atti Soc. Tosc. Sci. Nat., Mem., Serie A, 125 (2018)
pagg. 81-92, fig. 9; tab. 6; *doi: 10.2424/ASTSN.M.2018.25*

http://www.stsn.it/it/AttiA2018/marianellisupplmat.pdf

ANNA GATTI [1], PAOLA MARIANELLI [1], DANIELE ANDRONICO [2], ALESSANDRO SBRANA [1]

THE DECEMBER 2015 PAROXYSMS AT MT. ETNA: INSIGHTS FROM MINERAL CHEMISTRY AND GLASSES

Abstract - A. GATTI, P. MARIANELLI, D. ANDRONICO, A. SBRANA, *The December 2015 paroxysms at Mt. Etna: insights from mineral chemistry and glasses.*

In the last years, Mt. Etna was characterized by intense (explosive-effusive) eruptive activity. The December 2015 eruption was characterized by a quick sequence of eruptive episodes that produced eruption columns over 10 km in height, high lava fountains, Strombolian activity, persistent ash emissions and lava flows that involved four of the five summit craters in different moments. In this work, the juvenile fraction erupted during the paroxysmal phases occurred between 3 and 5 December 2015 was studied. In particular, we present mineralogical and compositional data of recognized mineral phases in the lapilli erupted during three of four explosive episodes and their melt inclusions and glassy groundmasses, aimed at a better understanding of the Mt. Etna plumbing system behavior and mainly related to the dynamics of its explosive eruptions.

Key words - Mt. Etna, paroxysm, mineral chemistry, melt inclusions.

Riassunto - A. GATTI, P. MARIANELLI, D. ANDRONICO, A. SBRANA, *L'eruzione parossistica dell'Etna del dicembre 2015: indicazioni sul comportamento del sistema di alimentazione dallo studio di minerali e vetri.*

Negli ultimi anni il vulcano Etna ha registrato un'intensa attività eruttiva, sia esplosiva che effusiva. L'eruzione dell'Etna del Dicembre 2015 è stata caratterizzata da una rapida sequenza di episodi eruttivi che ha generato colonne eruttive con altezze fino a 10 km, alte fontane di lava, attività stromboliana, colate laviche e persistenti emissioni di cenere, coinvolgendo quattro dei cinque crateri sommitali in momenti diversi. In questo lavoro è stata studiata la frazione juvenile eruttata durante le fasi parossistiche avvenute tra il 3 e 5 Dicembre 2015. In particolare vengono presentati dati mineralogici e composizionali delle fasi minerali, delle inclusioni silicatiche e dei vetri delle masse di fondo presenti nei lapilli eruttati durante tre di quattro episodi esplosivi, con l'obiettivo di dare un contributo alla comprensione del funzionamento del sistema di alimentazione dell'Etna, in relazione alla dinamica delle eruzioni esplosive.

Parole chiave - Monte Etna, parossismo, composizione chimica dei minerali, inclusioni silicatiche.

INTRODUCTION

Mt. Etna is a stratovolcano located in eastern Sicily, Italy, characterized by a long eruptive history subdivided into four main eruptive phases (e.g., Branca *et al*., 2011). The oldest phase (named *Basal Tholeiitic*) began ~500 ka ago in a shallow submarine environment (Gillot *et al*., 1994). The volcanism continued ~200 ka with increasingly more alkaline products (Armienti *et al*., 2004; *Timpe phase*). Since ~130 ka, the eruptive activity has taken place from the Valle del Bove area (a wide depression located in the east flank of the present volcano) up to the summit of the volcanic edifice (*Valle del Bove centres phase*). The fourth and last eruptive phase (named *Stratovolcano*) started ~57 ka ago. The continuous shifting of the activity to the NW initially built the largest volcanic center which represents the main bulk of the present edifice, i.e. the Ellittico volcano, where a composite caldera formed between ~15 and 19 ka due to four Plinian eruptions (Coltelli *et al*., 2000; Albert *et al*., 2013).

Since 15 ka, an intense and continuous effusive activity from both summit and flank vents gradually filled the Ellittico caldera and formed the Mongibello volcano. With time, eruptive fissures have frequently opened over the volcanic slopes along preferential trends or "rifts", exactly the NE, S and W rifts (Azzaro *et al*., 2012), which produced overlapping of lava flow fields and the growth of the Mongibello. Despite this huge effusive activity, several highly intense explosive eruptions from subplinian to Plinian also occurred, forming thick pyroclastic sequences (Coltelli *et al*., 2000).

The progressive increase of alkalinity and constant degree of differentiation of the lavas are the main feature of the trachybasalts erupted until today (Branca *et al*., 2004). However, in the last 30 years Mt. Etna displayed an apparent increase explosivity due to frequent paroxysmal eruptions (powerful Strombolian to lava fountaining activity). They occurred especially from the summit area, today consisting of five craters, i.e. North-East Crater (NEC), Voragine, Bocca Nuova, South-East Crater and New South-East Crater (NSEC). The last two have been the most active craters since 1998 producing together more than 200 paroxysmal episodes (Andronico *et al*., 2015; Corsaro *et al*., 2017).

According to Acocella *et al*. (2016) and references therein, in the last decades two main stress conditions have controlled the overall evolution of the summit

[1] Dipartimento di Scienze della Terra, Università di Pisa, via S. Maria 53, 56126 Pisa, Italy. *Corresponding author e-mail*: paola.marianelli@unipi.it
[2] Istituto Nazionale di Geofisica e Vulcanologia, Sezione di Catania, Osservatorio Etneo, Piazza Roma 2, 95125 Catania, Italy.

fracture field at Mt. Etna. The first condition corresponds to the presence of the stationary extensional stress field acting on the longer-term both at the base and the summit of the volcano, and produced an overall E-W extension on the volcano summit. This condition was active until a period between 2001 and 2004, during which it was replaced by the second stress condition, characterized by an overall NE-SW trending extension direction. This second condition is invoked for the development of related feeder dikes which propagated from the SEC and resulted into the build-up of the NSEC.

In early December 2015, an extraordinary sequence of eruptive events occurred from four of five summit craters in few days (Corsaro *et al.*, 2017). In recent years, eruptive activities at two or three different craters were observed almost coevally only during the 1997, 1998 and 1999 eruptions (Harris & Neri, 2002; Behncke *et al.*, 2003; Calvari *et al.*, 2003; Corsaro *et al.*, 2013). However, in 2015 such a close activity occurred i) much more rapidly (2 weeks), ii) from a higher number of craters, and finally iii) producing some very powerful explosive eruptions.

In 2015, between the early hours of 3 December and the afternoon of 5 December, the Voragine crater produced four lava fountaining episodes (hereafter I, II, III and IV, respectively; Table 1), the first of which possibly took place temporarily also from the Bocca Nuova (Fig. 1a). Magma jets reached several hundred meters above the vent (Fig. 1a), while eruption columns containing ash, lapilli and bombs rose up to 10-14 km above sea level (Fig. 1b; Vulpiani *et al.*, 2016; Corsaro *et al.*, 2017). Abundant, incandescent magma fragments fell down the Voragine and Bocca Nuova craters, forming rheomorphic lava flows which filled these craters without overflowing their rims; interestingly, these deposits rapidly subsided in the following months (Corsaro *et al.*, 2017). Few days later, the NSEC produced Strombolian and effusive activity (6-8 December), while ash emissions occurred also from the NEC and declined after 9 December before their cessation on 13 December (Corsaro *et al.*, 2017).

In this paper, we study the tephra erupted during three of the four episodes of lava fountain at the Voragine.

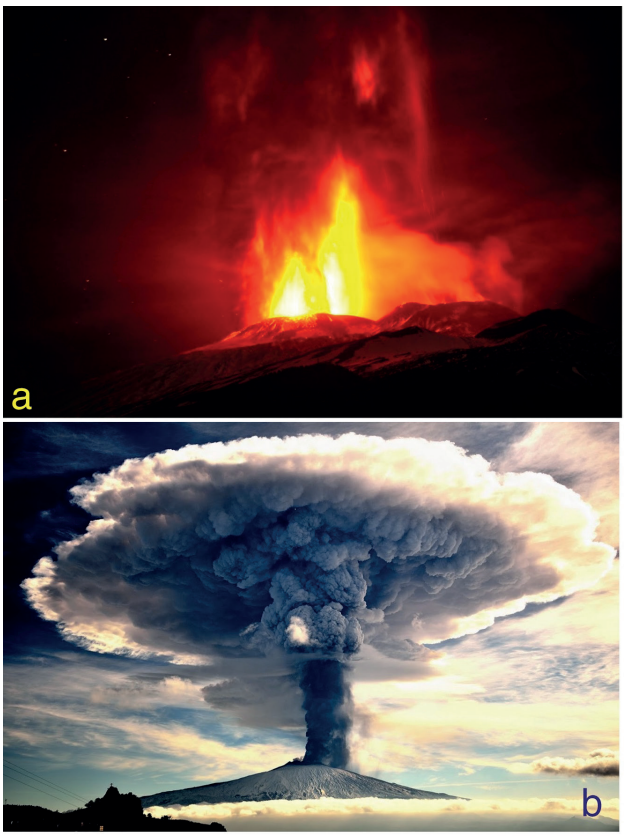

Fig. 1 - Images of the 2015 December paroxysmal eruptions at Mt. Etna: a) lava fountaining activity viewed from SW in the night of 3 December 2015 (episode I). The two lava jets rising from the summit area suggest the involvement of both Voragine and Bocca Nuova craters (on the left and right, respectively). Photo courtesy of Francesco Ciancitto; b) the exceptional eruption column formed above the volcano in the morning of 4 December 2015 (episode II) photographed in the village of Cesarò, at 27 km NW from the summit. Photo courtesy of Giuseppe Famiani.

The bulk rock composition of the products erupted during the episodes I and II has been done by Corsaro *et al.* (2017), while Pompilio *et al.* (2017) carried out a combined textural and compositional study on ash-sized volcanic particles of three of the four tephra deposits. Here, we focus in particular on the character-

Table 1 - The four lava fountain episodes of 3-5 December 2015 at Voragine; tephra dispersal and coordinates (UTM) of the samples collected for this work are also reported. Data on the duration of the paroxymal phase (i.e. lava fountaining activity) are from Corsaro et al. (2017).

Date	Episode number	Paroxysm duration		Tephra dispersal	Samples	Coordinates (UTM)	
		start	end			X	Y
3 December	I	02:20	03:10	NE	1	503602.65	4182351.00
4 December	II	09:05	10:10	E			
4 December	III	20:25	21:05	NE	1	503602.65	4182351.00
5 December	IV	14:45	15:35	W	2	499548.11	4177388.24

ization of magma involved in the Voragine eruptions throughout microanalysis of phenocrysts and glasses (groundmass and melt inclusion) of juvenile lapilli.
Although pyroclasts and lava flow erupted from the Voragine and NSEC are K-trachybasalts, according to Corsaro *et al.* (2017), in December 2015 the summit craters erupted different magmas. Based on the petrographic and chemical characteristics of the juvenile products, the magma batches erupted on episodes I and II at Voragine were stored at shallow depth, while the most primitive magma of the eruptive period was erupted at the NEC on December 6. This compositional framework suggests that the samples studied in this work can get new insight into the eruptive processes driving lava fountains at Mt. Etna and, in particular, into the shallow plumbing system feeding the Voragine crater during the 2015 paroxysmal sequence.

Analytical Methods

In this work, juvenile lapilli were crushed and sieved, using 4 mm, 2 mm, 1 mm and 0.75 mm squared-mesh sieves. Phenocrysts were hand-picked from < 1 mm and <0.75 mm fraction using a stereomicroscope. The selected crystals were mounted on glass slides and polished. EDS analyses were performed on phenocrysts and on glassy groundmass. Through accurate petrographic inspection, glassy melt inclusions were selected and prepared for microanalysis.
Mineral phases and silicate melt inclusions composition was determined with SEM-EDS at Earth Science Department of Pisa University. The used equipment consists of a scanning electron microscope Philips XL30 with a quantitative microanalysis system EDAX-DX4. Operating conditions were 20 kV accelerating voltage, 0.1 nA beam current, 200-500 nm spot diameter and 100 seconds live time. For the glass analysis a scanning area of 100 μm^2 was used in order to mitigate the loss of light elements by diffusion effect. Each analytic session was preceded by calibration and analyses of certified minerals and natural glasses standard (basaltic glass ALV981R23 and trachyitic glass CFA47). The analytical error is minor of 1% for concentrations higher than 15 wt%, 2% for 5-15 wt%, 5% for 1-5 wt%, and 30% for <1 wt%; see Marianelli & Sbrana, 1998 and Appendix A for standard analyses performed during analytical sessions).

Studied Samples

In this work, we studied two tephra samples erupted during the fountaining activity at the Voragine and consisting of lapilli in the dimensional range of ~1-4 cm.
Sample 1 was collected at 5-6 km of distance from the Voragine in the NE slope of Mt. Etna, where the fallout deposits of lava fountains I and III (occurred early in the morning of 3 December and late in the afternoon of 4 December, respectively) overlapped. Hence, lapilli as well as analytical results from sample 1 represent both deposits being indistinguishable each other.
Sample 2 contains lapilli erupted during the lava fountain episode IV on 5 December afternoon, and it was collected within ~1 km SW from the Voragine.
The duration of the paroxysmal phase (i.e. the phase of the lava fountain during which an eruption column forms above the crater and disperses bombs, lapilli and ash up to tens of kilometers of distance; Alparone *et al.*, 2003) is almost similar (50 min, 40 min and 50 min, respectively) for the three studied events (Corsaro *et al.*, 2017).

Results

Lapilli from both samples show homogeneous petrographic features, with porphyricity index ranging from 20% to 25% for samples erupted during episodes I and III (Corsaro *et al.,* 2017).
Sample 1 is macroscopically characterized by a minor amount of phenocrysts in respect to sample 2. In both samples in order of abundance plagioclase, clinopyroxene, olivine and opaque minerals occur either as phenocrysts and groundmass microlites. Lapilli groundmass shows variable microlite content, ranging from poorly to highly crystallized clasts, as already described by Pompilio *et al.* (2017). In order to have information on melt present in the feeding system at the time of eruption, glassy groundmass analyses were performed only on microlite-free lapilli ("poorly crystallized clasts" of Pompilio *et al.*, 2017).

Mineral Chemistry

Plagioclase is the more abundant phenocryst, with irregular shape and color variations ranging from light to dark brown, generated by the high concentration of cryptocrystalline inclusions; these inclusions are particularly settled in the core. Plagioclase compositions range from Bytownite to Labradorite (Fig. 2 and Table 2).
Clinopyroxene crystals present a regular prismatic shape, dark green colored with c-axis parallel cleavage. In both samples their composition is diopsidic (Fe-rich diopside). Ferrosilite content range between 8.8 wt% and 14.6 wt% (Fig. 3 and Table 3).
Olivine crystals are generally sub-rounded and contain glassy inclusions and opaque minerals. Studied olivines show Forsterite composition from 82 wt%

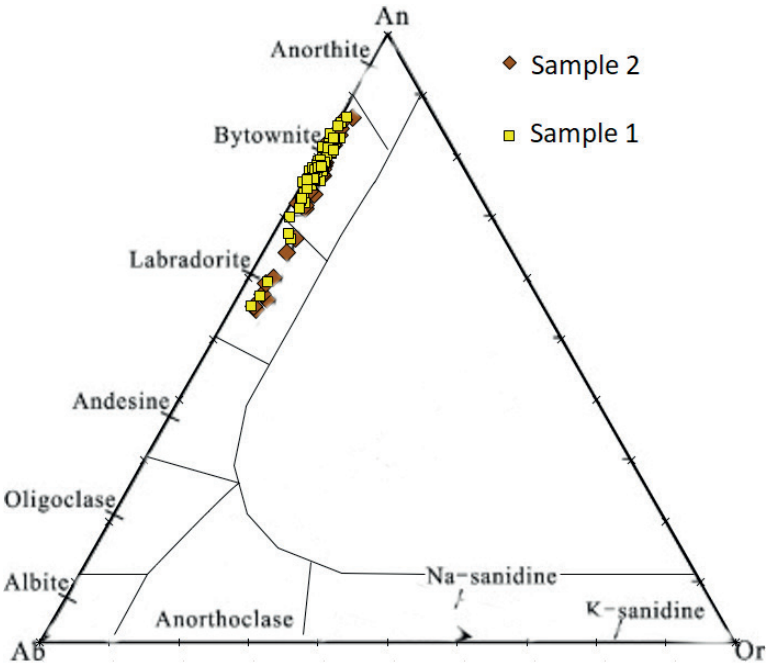

Fig. 2 - Compositional diagram of plagioclases.

Table 2 - Selected EDS analyses of plagioclase.

	1F An57 sample 1	5N An174 sample 1	6N An195 sample 1	4N An107 sample 1	9C An264 sample 2	11O An409 sample 2	11M An405 sample 2	11L An403 sample 2
SiO_2	52.81	53.08	44.84	44.5	53.18	52.8	44.67	44.44
Al_2O_3	29.41	29.85	35.02	34.94	29.2	29.91	35	35.07
FeO	0.72	0.23	0.35	0.48	0.55	0.16	0.53	0.33
CaO	11.9	11.54	18.16	18.32	11.56	12	18.14	18.34
Na_2O	4.58	4.82	1.47	1.64	4.84	4.55	1.54	1.61
K_2O	0.57	0.47	0.16	0.12	0.67	0.58	0.12	0.22
An	57.0	55.4	86.4	85.5	54.7	57.4	86.1	85.2
Ab	39.7	41.9	12.7	13.9	41.5	39.4	13.2	13.5
Or	3.3	2.7	0.9	0.7	3.8	3.3	0.7	1.2

to 68 wt% (Table 4); crystals although with variable composition do not present chemical zoning. Fo-rich olivines are more abundant in Sample 2 (Fig. 4).

Melt Inclusions and Glassy Groundmass

Melt inclusions (MIs) are present in all the mineral phases of both samples, showing size ranging from 10 µm to 100 µm, and shapes ranging from sub-spherical to stretched (Fig. 5 and Fig. 6). Most of the inclusions are two-phases, with glass and shrinkage bubbles, while rare MIs are a single phase (brown glass) without shrinkage bubble or impurity. Few MIs have petrographic textures (such as jagged edges or small crystals on the walls of the shrinkage bubble; Fig. 6b, e, f) suggesting after-trapping evolution. For this reason, these MIs were disregarded for microanalysis and only the larger glassy MIs, together glassy groundmass were analyzed for major elements.

All of the MIs (Table 5) and glassy groundmass (Table 6 and Fig. 6g, h) analysis for each sample were reported in a TAS diagram (Le Maitre *et al.*, 2002). Glassy matrix of both samples is phonotephritic, but some basaltic-trachyandesitic composition are present in Sample 2. MIs in Sample 1 shows a wide compo-

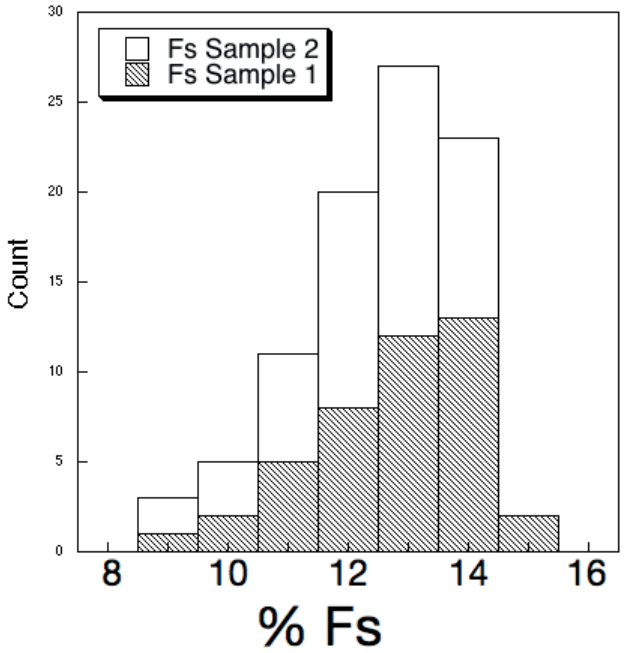

Fig. 3 - Histogram showing Ferrosilite (mol%Fs) contents in clinopyroxene for sample 1 and sample 2.

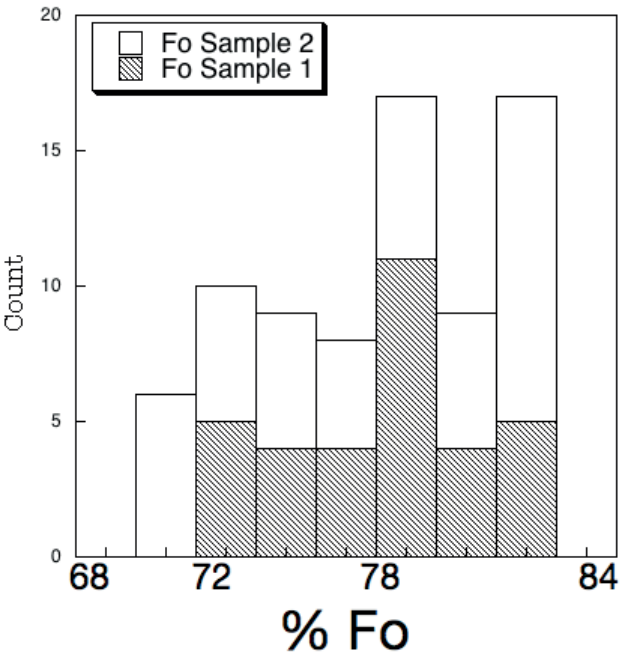

Fig. 4 - Histogram showing forsterite (mol %Fo) contents in olivine for sample 1 and sample 2.

Table 3 - Selected EDS analyses of clinopyroxene.

	1A An15 sample 1	2G An34 sample 1	2I An38 sample 1	5I An168 sample 1	9N An282 sample 2	10M An386 sample 2	9I An277 sample 2
SiO_2	47.24	48.36	49.50	49.85	47.30	49.38	49.36
TiO_2	1.97	1.55	0.92	0.97	2.13	0.93	0.64
Al_2O_3	6.58	4.79	4.08	4.50	5.75	3.97	4.51
FeO	8.51	8.91	6.15	5.58	8.68	5.58	6.03
MnO	0.07	0.25	0.16	0.07	0.22	0.10	0.09
MgO	13.03	13.21	15.70	16.03	12.82	15.93	15.68
CaO	22.24	22.27	22.97	22.39	22.50	23.27	22.95
Na_2O	0.36	0.66	0.37	0.53	0.60	0.64	0.57
Wo	47.3	46.8	46.3	45.7	47.8	46.7	46.4
En	38.6	38.6	44.0	45.5	37.9	44.2	44.1
Fs	14.13	14.61	9.67	8.88	14.38	8.75	9.51

Table 4 - Selected EDS analyses of olivine.

	2F An32 sample 1	1E An53 sample 1	4P An109 sample 1	13N An494 sample 2	8C An240 sample 2	13H An490 sample 2
SiO_2	38.24	38.24	37.79	39.13	39.71	39.11
FeO	23.33	24.12	24.69	18.15	16.21	16.96
MnO	0.53	0.83	0.88	0.41	0.47	0.52
MgO	37.42	36.22	36.26	41.89	43.29	43.05
CaO	0.48	0.59	0.38	0.42	0.32	0.36
Fo %	74.1	72.8	72.4	80.5	82.6	81.9

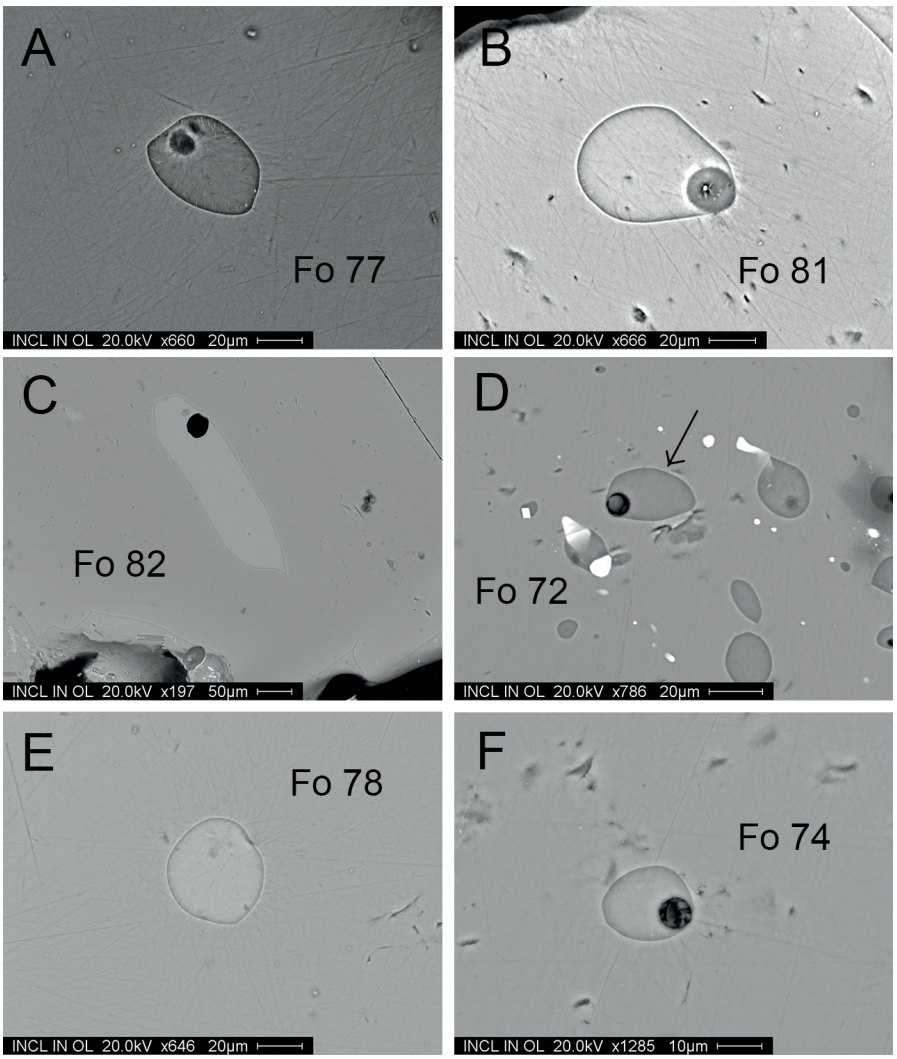

Fig. 5 - Backscattering images of MIs with size from 10 to 50 µm and variable shape, hosted in different olivine crystals belonging to the sample 1: a) An.144, 4F; b) An.207, 5E; c) An.221, 6F; d) An.222, 6H indicated with the arrow; e) An.122, 3G; f) An.128, 3M.

sitional range from trachybasalt to phonotephrites. Sample 2 MIs compositional range is similar, but phonotephritic compositions are more abundant (Fig. 7). A few MIs hosted in olivine have more primitive compositions than the MIs hosted in clinopyroxene and plagioclase and the glassy matrix (Fig. 7).

Discussion

Tephra samples related to the paroxysmal activity at Voragine on December 2015 were already studied by Corsaro *et al.* (2017) and Pompilio *et al.* (2017). In this paper, new analytical data about the chemical composition of minerals, residual glasses and MIs were carried out on two tephra samples representative of three of four lava fountains. Glassy matrix of poorly crystalline clasts (Fig. 6h) have basaltic-trachyandesite to phonotephrite compositions, well in agreement with data from recent eruptions (Fig. 7) and partly overlapping composition of glassy matrix of poorly crystalline clasts (PC analyses reported by Pompilio et al., (2017). Differences between data of the present paper and literature data are not attributable to analytical errors (cfr Appendix A for quality of this paper's EDS analyses). Heterogeneity of samples studied by different authors cannot be excluded, anyway we have to remark that such differences would be minimized if also literature analyses were normalized to 100 before their plotting in TAS diagram of Fig. 7.
Mineral chemistry of phenocrysts is quite homogeneous for the two samples, only olivine composition shows some inhomogeneities. Olivine crystals occur as unzoned phenocrysts with different compositions. In fact, the frequency plot of Fo% in Fig. 4 highlights the presence of at least 2 groups of olivine

Table 5 - Selected compositions of MIs in olivine crystals.

	3G An122 sample 1	3M An128 sample 1	4F An144 sample 1	5E An207 sample 1	6F An221 sample 1	6H An222 sample 1	8C An290 sample 2	13N An528 sample 2	13N An529 sample 2	12D An501 sample 2	13B An512 sample 2	13D An516 sample 2
Analyzed compositions												
SiO_2	46.25	46.25	49.37	49.21	45.62	51.3	45.78	46.6	45.52	47.24	46.14	47.22
TiO_2	1.84	1.89	1.87	1.94	1.87	1.47	1.97	2.06	2.02	1.8	2.14	1.98
Al_2O_3	18.58	18.31	17.64	18.3	18.55	17.43	16.13	16.37	17.1	17.42	17	17.86
FeO_{tot}	9.45	10.29	9.97	9.49	9.34	9.52	12.08	10.7	10.57	10.7	10.61	10.45
MnO	0.22	0.22	0.26	0.14	0.07	0.2	0.27	0.13	0.28	0.26	0.25	0.16
MgO	4.12	2.99	3.66	2.9	4.65	2.44	3.86	6.2	5.25	4.83	5.91	4.27
CaO	12.74	13.64	9.54	10.19	13.28	9.69	13.56	12.03	12.92	11.31	11.86	10.49
Na_2O	3.89	3.58	4.65	4.88	3.88	4.82	3.44	3.19	3.24	3.82	3.03	4.72
K_2O	2.14	1.95	2.39	2.36	2.13	2.37	1.88	2.03	2.14	1.98	2.22	2.38
P_2O_5	0.22	0.22	0.37	0.27	0.25	0.27	0.39	0.12	0.44	0.18	0.26	0.29
S	0.36	0.4	0.14	0.19	0.31	0.21	0.38	0.36	0.38	0.32	0.42	0.1
Cl	0.19	0.25	0.14	0.15	0.06	0.28	0.26	0.19	0.14	0.14	0.16	0.09
Restored compositions												
SiO_2	45.86	45.82	48.80	48.26	45.23	50.61	45.33	46.47	45.21	47.08	45.82	46.44
TiO_2	1.75	1.80	1.78	1.76	1.76	1.40	1.87	2.04	1.94	1.78	2.05	1.80
Al_2O_3	17.67	17.42	16.78	16.61	17.48	16.58	15.33	16.19	16.42	17.22	16.32	16.21
FeO	8.64	9.54	9.16	8.94	8.50	8.94	11.01	9.41	9.48	9.44	9.47	9.58
Fe_2O_3	1.38	1.52	1.46	1.43	1.36	1.43	1.76	1.50	1.51	1.51	1.51	1.53
MnO	0.21	0.21	0.25	0.13	0.07	0.19	0.29	0.13	0.28	0.26	0.25	0.18
MgO	5.88	4.61	5.37	6.47	6.83	4.05	5.46	6.54	6.65	5.16	7.33	7.81
CaO	12.14	12.99	9.09	9.28	12.53	9.24	12.91	11.90	12.42	11.18	11.40	9.56
Na_2O	3.70	3.41	4.42	4.43	3.66	4.59	3.27	3.15	3.11	3.78	2.91	4.28
K_2O	2.04	1.85	2.27	2.14	2.01	2.25	1.79	2.01	2.05	1.96	2.13	2.16
Tot.	100	100	100	100	100	100	100	100	100	100	100	100
K_D	0.31	0.31	0.31	0.30	0.30	0.31	0.31	0.30	0.30	0.31	0.30	0.31
% Olivine	5	5	5	10	6	5	5	1	4	1	4	10
%Fo	79.7	73.7	77.2	81.0	82.6	72.5	82.6	80.5	80.5	76.0	82.2	82.6
K_2O/Al_2O_3	0.12	0.11	0.14	0.13	0.11	0.14	0.12	0.12	0.13	0.11	0.13	0.13
CaO/Al_2O_3	0.69	0.75	0.54	0.56	0.72	0.56	0.84	0.74	0.76	0.64	0.69	0.58

Footnote: $K_D=[(FeO/MgO)_{ol}/(FeO/MgO)_{melt}]$ after recalculation; post-entrapment crystallization on the MI walls (PEC %) (see text).

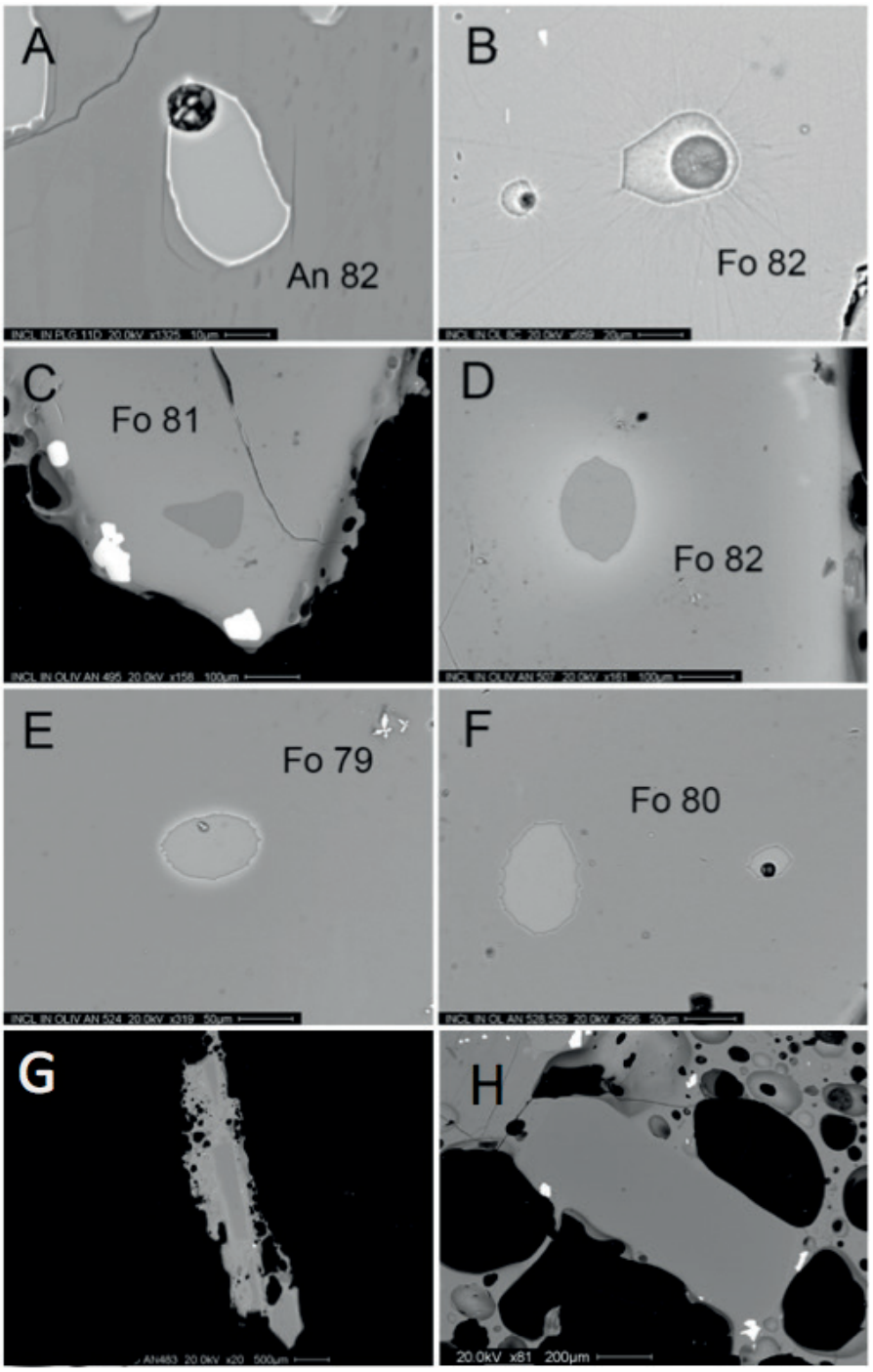

Fig. 6 - Backscattering images of MIs with size from 10 to 100 µm and variable shape, hosted in different olivine crystals and a plagioclase crystal belonging to the sample 2: a) An.448, 11D in plagioclase; b) An.290, 8C; c) An.495, 12A; d) An.507, 12G; e) An.524, 13I; f) An.528 left and An.529 to the right, 13M; g) An.483 13C olivine and poorly crystalline glassy groundmass; h) olivine An.4 and poorly crystalline glassy groundmass.

("Fo<78"and "Fo>82" populations), that can be related to 3 (mm1, MM1 and MM0) of the three olivine populations identified by Kahl *et al.* (2015) for the 1991-2008 magma plumbing system of Mt. Etna. In particular, the high-Fo composition is more abundant in Sample 2, in agreement with the slightly lower Fs content of clinopyroxenes from this sample. The different compositions and the lacking of compositional zoning that characterize olivine could be ascribed to a magma mixing process (syn-eruptive, without the time required for re-equilibration of growing crystals) and/or to the occurrence of crystals from the mush hosted in Mt. Etna plumbing system (cognate xenocrystals), possibly because the erosive action of the gas flux and

Table 6 - Selected EDS analyses of glassy groundmass in microlite-poor clasts.

	An1 sample 1	An2 sample 1	An3 sample 1	An7 sample 2	An8 sample 2	An9 sample 2
SiO_2	48.80	49.67	50.25	50.54	50.43	50.32
TiO_2	2.00	2.06	2.10	1.98	2.13	1.96
Al_2O_3	17.37	17.25	17.19	17.28	17.27	17.31
FeOtot	9.49	10.30	10.27	9.84	9.91	9.75
MnO	0.24	0,30	0,25	0,00	0,16	0,19
MgO	4.23	3.49	3.28	3.56	3.62	3.46
CaO	7.64	8.04	8.28	8.19	8.16	8.05
Na_2O	5.77	4.92	4.51	5.11	4.54	5.00
K_2O	3.99	3.44	3.48	3.21	3.36	3.48
P_2O_5	0.48	0.52	0.38	0.29	0.42	0.46
K_2O/Al_2O_3	0.23	0.20	0.20	0.19	0.19	0.20
CaO/Al_2O_3	0.44	0.47	0.48	0.47	0.47	0.47

opening of various magma pathway, according to Kahl *et al.* (2015).

Some olivine-hosted MIs show petrographic evidences of post-trapping crystallization of olivine on cavity walls (Fig. 6). For this reason, analyses of olivine-hosted MIs were corrected for post-trapping evolution by simulating reverse olivine fractionation using the model of Ford *et al.* (1983); the Fe3+/Fe2+ ratio in the melt is calculated following Borisov (1989) and assuming fO_2 close to the NNO buffer (Métrich & Clocchiatti, 1996). Recalculation stopped when K_D for MIs hosted in olivine ($K_D=[(FeO/MgO)_{ol}/(FeO/MgO)_{melt}]$) reach values comparable with the range 0.30-0.29 reported by Métrich *et al.* (2004) indicating the achievement of the olivine-melt equilibrium (Roedder & Emslie, 1970). Therefore, the restored compositions can be assumed representative of melt at the time of trapping, although care must be taken for MIs compositions with higher (>6%) post trapping evolution. These latter show a worse correlation with host olivine composition (Fo content), so we can speculate that some unrecoverable modifications affect these MIs, therefore their recalculated compositions could not be strictly representative of the trapped melts.

For each sample, MIs and glassy groundmass analyses were reported in a K_2O/Al_2O_3 vs CaO/Al_2O_3 diagram (Fig. 8). Both MIs and glassy matrix show relatively homogeneous compositions with a K_2O/Al_2O_3 value in the range 0.3 to 0.1 and a CaO/Al_2O_3 ratio ranging from 0.3 to 0.6 for most of data. Some clinopyroxene and plagioclase-hosted MIs have more differentiated compositions (lower CaO/Al_2O_3) than glassy matrix. Only MIs in olivine and some MIs in clinopyroxene reach less evolved compositions ($CaO/Al_2O_3 < 0.6$; Fig. 8).

A good agreement can be observed between most of MIs and glassy matrix compositions (Fig. 8). This makes us confident that host crystals are in equilibrium with hosting silicate melt present in the feeding system at the time of eruption. This assumption is supported also by the petrographic features of most of MIs, characterized by absence of negative shapes of cavity and their clean glassy appearance. Evidences of an involvement of a slightly more primitive magma derive from the occurrence of some high CaO/Al_2O_3 (Fig. 8) ratio in some olivine and clinopyroxene crystals (CaO/Al_2O_3 up 0.85 found in sample 2 involved in the lava fountain episode IV).

As MIs composition can be assumed as representative of melt in equilibrium with host crystal at the time of trapping, the different populations of olivine could be ascribed to two different steps of crystallization (according to Kahl *et al.* 2015 and references therein), and in this view the study of MIs hosted in such phenocrysts could provide information about the evolution of the Etnean plumbing system in pre-eruptive conditions. However, we cannot exclude that few relatively evolved compositions in Sample 2 (Table 5) could be ascribed to embayment of melt instead of trapping of true MIs, although the petrographic inspection of samples before polishing and analyses seems to exclude this possibility. In both samples, the amount of post-trapping crystallization of host crystals correlates with the Fo content of olivine (Fig. 9). Low-Fo ("Fo<78" group) and some Fo-rich ("Fo>82" group) crystals contain MIs with no post-entrapment

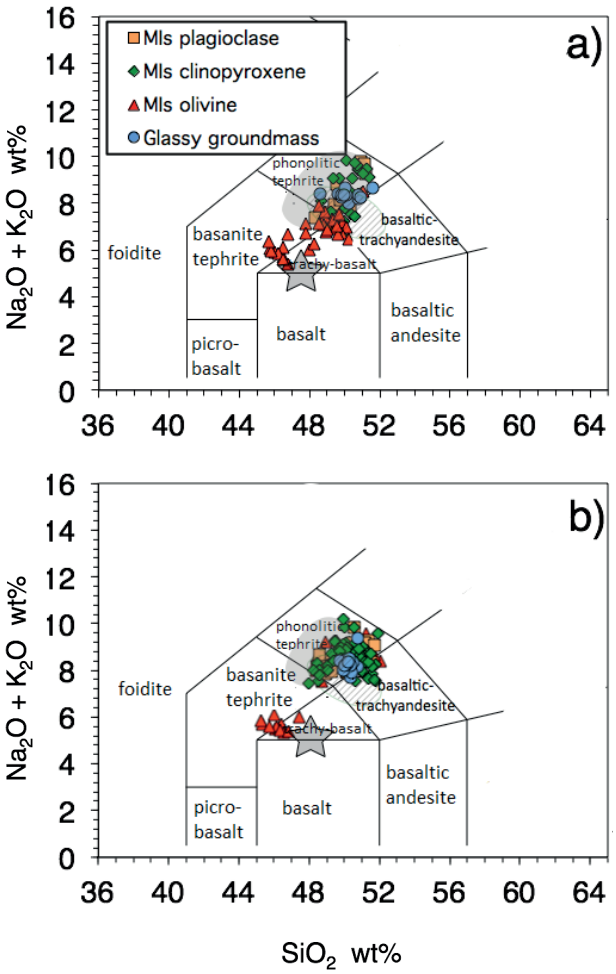

Fig. 7 - TAS diagram for glassy melt inclusions hosted in olivine, clinopyroxene and plagioclase, and glassy matrix: a) sample 1 and b) sample 2. Grey area represents composition of glass in tephra from recent eruptions of Mt. Etna (data from Corsaro & Pompilio, 2004 and form Taddeucci et al., 2004). Dashed field represents glasses from poorly crystallized clasts (data from Pompilio et al., 2017); note that in the present paper literature analyses are plotted in the TAS diagram after normalizing to 100 for comparison, so the dashed field results shifted in respect to those defined in Figure S4 of Pompilio et al. (2017). Bulk rock (data form Corsaro et al. 2017) is also reported (grey star).

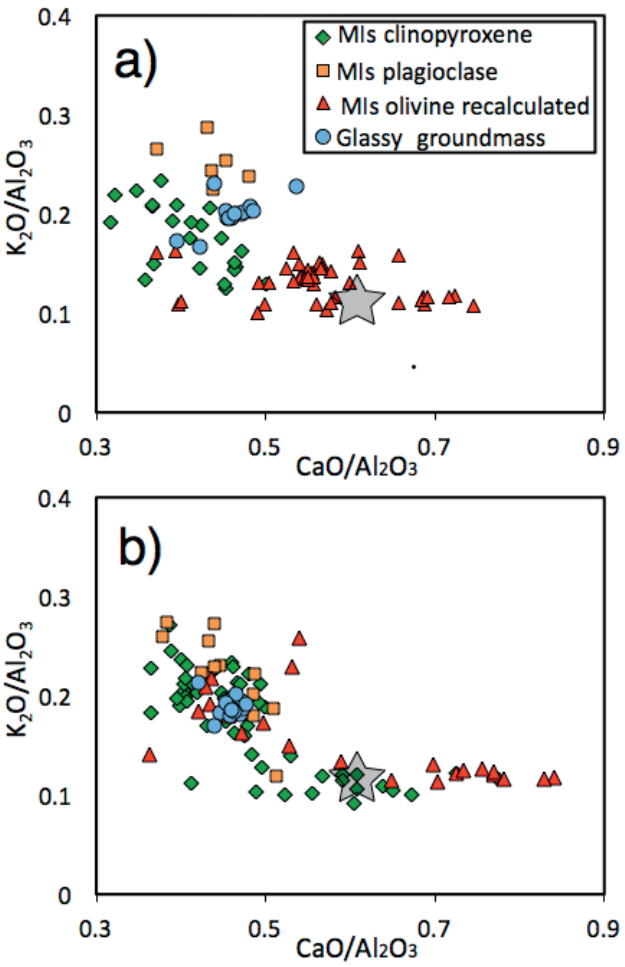

Fig. 8 - Composition of MIs hosted in olivine, clinopyroxene and plagioclase, and of glassy groundmass reported in a CaO/Al_2O_3 vs K_2O/Al_2O_3 diagram: a) sample 1 and b) sample 2. Compositions of olivine hosted MIs are recalculated (see text). Bulk rock (data form Corsaro et al. 2017) is also reported (grey star).

der, 1984), and the occurrence of MIs with high CaO/Al_2O_3 ratios which are trapped in olivine ~Fo82 but also in olivine Fo73.7 (Table 5).

Conclusions

Our work allows further insights about the Mt. Etna plumbing system during the December 2015 eruptive period, in particular about processes affecting eruption from Voragine crater, through the characterization of the mineral phases.

According to Corsaro *et al.* (2017), the magma composition indicates that the eruptive activity of December 2015 represents the climax of an unrest initiated in January 2015, with episodic magma supplies of the volcano's shallow plumbing system. At the beginning of November, a more consistent recharge of volatile-rich and more primitive magma formed a deeper zone of the shallow plumbing system. This batch enhanced the Strombolian activity at the Voragine crater and culminated with the four paroxysms of early December which discharged a K-trachybasaltic magma already present in the shallow plumbing system of the volcano. Furthermore, even the paroxysmal phase is supposed to be related to the eruption of a trachybasaltic magma already present in the shallow plumbing system, which

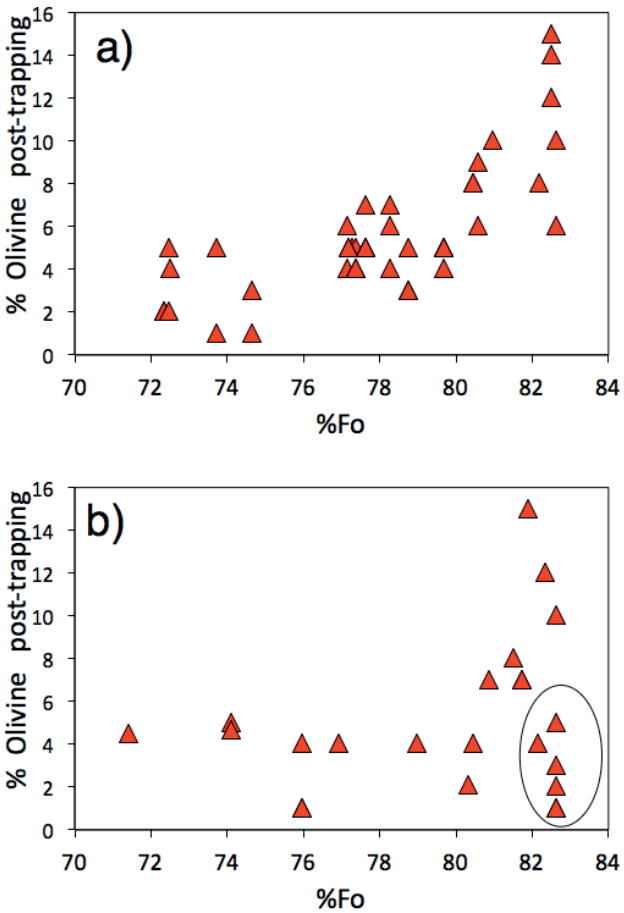

Fig. 9 - Diagram showing the relationship between the recalculated MIs in olivine and the %Fo content of host mineral: a) sample 1 and b) sample 2. In b) MIs enclosed in circle represent the "Fo>82 group" with minor evidences of post trapping evolution.

was however refilled by a more primitive volatile-rich magma (Corsaro *et al*., 2017) from deeper zone (Kahl *et al*., 2015). This hypothesis is supported by the juvenile fraction features of the lava fountains I and III on 3-4 December compared to the features of the juvenile fraction emitted by the fourth and last lava fountain on 5 December; in particular, the presence of Fo-richer olivine crystals and some MIs with high CaO/Al_2O_3 values recorded in Sample 2 and highlighted in this paper.

AKNOWLEDGEMENTS

This work was financially supported by the University of Pisa through Ateneo 2017 funds. Francesco Ciancitto and Giuseppe Famiani are thanked for sharing their photographs in Figures 1a and 1b. The authors are grateful to Patrizia Landi, to Nicole Métrich and to an anonymous reviewer for their constructive comments, suggestions and criticisms that greatly helped to improve the quality of the manuscript.

REFERENCES

ACOCELLA V., NERI M., BEHNCKE B., BONFORTE A., DEL NEGRO C., GANCI G., 2016. Why Does a Mature Volcano Need New Vents? The Case of the New Southeast Crater at Etna. *Frontiers in Earth Science* 4: 67.

ALBERT P.G., TOMLINSON E.L., LANE C.S., WULF S., SMITH V.C., COLTELLI M., KELLER J., LO CASTRO D., MANNING C.J., MUELLER W., MENZIES M.A., 2013. Late glacial explosive activity on Mount Etna: Implications for proximal-distal tephra correlations and the synchronisation of Mediterranean archives. *Journal of Volcanology and Geothermal Research* 265: 9-26.

ALPARONE S., ANDRONICO D., LODATO L., SGROI T., 2003. Relationship between tremor and volcanic activity during the Southeast Crater eruption on Mount Etna in early 2000. *Journal of Geophysical Research: Solid Earth* 108(B5): 2241.

ANDRONICO D., SCOLLO S., CRISTALDI, A., 2015. Unexpected hazards from tephra fallouts at Mt Etna: The 23 November 2013 lava fountain. *Journal of Volcanology and Geothermal Research* 304: 118-125.

ARMIENTI P., TONARINI S., D'ORAZIO M., INNOCENTI F., 2004. Genesis and evolution of Mt. Etna alkaline lavas: petrological and Sr-Nd-B isotope constraints. *Periodico di Mineralogia* 73: 29-52.

AZZARO R., BRANCA S., GWINNER K., COLTELLI M., 2012. The volcano-tectonic map of Etna volcano, 1: 100.000 scale: an integrated approach based on a morphotectonic analysis from high-resolution DEM constrained by geologic, active faulting and seismotectonic data. *Italian Journal of Geosciences* 131: 153-170.

BEHNCKE B., NERI M., CARNIEL R., 2003. An exceptional case of endogenous lava dome growth spawning pyroclastic avalanches: the 1999 Bocca Nuova eruption of Mt. Etna (Italy). *Journal of Volcanology and Geothermal Research* 124: 115-128.

BORISOV A.A., 1989. New empirical equation of dependence of the Fe3+/ Fe2+ ratio in natural melts on their composition, oxygen fugacity and temperature. *Geokhimiya* 6: 892-897.

BRANCA S., COLTELLI M., GROPPELLI G., 2004. Geological evolution of Etna volcano. *Etna Volcano Laboratory, Bonaccorso, Calvari, Coltelli, Del Negro, Falsaperla (Eds), AGU (Geophysical monograph)* 143: 49-63.

BRANCA S., COLTELLI M., GROPPELLI G., 2011. Geological evolution of a complex basaltic stratovolcano: Mount Etna, Italy. *Italian Journal of Geosciences* 130: 306-317.

CALVARI S., NERI M., PINKERTON H., 2003. Effusion rate estimations during the 1999 summit eruption on Mount Etna, and growth of two distinct lava flow fields. *Journal of Volcanology and Geothermal Research* 119: 107-123.

COLTELLI M., DEL CARLO P., VEZZOLI L., 2000. Stratigraphic constraints for explosive activity in the last 100 ka at Etna volcano, Italy. *International Journal of Earth Sciences* 89: 665-677.

CORSARO R.A., ANDRONICO D., BEHNCKE B., BRANCA S., CALTABIANO T., CIANCITTO F., MIRAGLIA L., 2017. Monitoring the December 2015 summit eruptions of Mt. Etna (Italy): Implications on eruptive dynamics. *Journal of Volcanology and Geothermal Research* 341: 53-69.

CORSARO R.A., DI RENZO V., DI STEFANO S., MIRAGLIA L., CIVETTA L., 2013. Relationship between petrologic processes in the plumbing system of Mt. Etna and the dynamics of the eastern flank from 1995 to 2005. *Journal of Volcanology and Geothermal Research* 251: 75-89.

FORD C.E., RUSSEL D.G., CRAVEN J.A., FISK M.R., 1983. Olivine liquid equilibria: temperature, pressure and composition dependence of the crystal/liquid cation partition coefficients for Mg,Fe2+, Ca, Mn. *Journal of Petrology* 24: 256-265.

GILLOT P.Y., KIEFFER G., ROMANO R., 1994. The evolution of Mount Etna in the light of potassium-argon dating. *Acta Vulcanologica* 5: 81-87.

HARRIS A.J., NERI M., 2002. Volumetric observations during paroxysmal eruptions at Mount Etna: pressurized drainage of a shallow chamber or pulsed supply? *Journal of Volcanology and Geothermal Research* 116: 79-95.

KAHL M., CHAKRABORTY S., POMPILIO M., COSTA F., 2015. Constraints on the nature and evolution of the magma plumbing system of Mt. Etna Volcano (1991-2008) from a combined thermodynamic and kinetic modelling of the compositional record of minerals. *Journal of Petrology* 56: 2025-2068.

LE MAITRE R.W., STRECKEISEN A., ZANETTIN B., LE BAS M.J., BONIN B., BATEMAN P., 2002. Igneous rocks: a classification and glossary of terms: recommendations of the International Union of Geological Sciences Subcommission on the Systematics of Igneous Rocks. *Bulletin of the Volcanological Society of Japan* 51.4: 211-229.

MARIANELLI P., SBRANA A., 1998. Risultati di misure di standard di minerali e di vetri naturali in microanalisi a dispersione di energia. *Atti Società Toscana Scienze Naturali, Memorie Serie A* 105: 57-63.

MÉTRICH N., ALLARD P., SPILLIAERT N., ANDRONICO D., BURTON M., 2004. 2001 flank eruption of the alkali-and volatile-rich primitive basalt responsible for Mount Etna's evolution in the last three decades. *Earth and Planetary Science Letters* 228: 1-17.

MÉTRICH N., CLOCCHIATTI R., 1996. Sulfur abundance and its speciation in oxidized alkaline melts. *Geochimica et Cosmochimica Acta* 60: 4151-4160.

POMPILIO M., BERTAGNINI A., DEL CARLO P., DI ROBERTO A., 2017. Magma dynamics within a basaltic conduit revealed by textural and compositional features of erupted ash: the December 2015 Mt. Etna paroxysms. *Scientific Reports* 7: 4805.

ROEDDER E., 1984. Fluid inclusions. Review in Mineralogy. 644 pp.

ROEDER P.L., EMSLIE R.F., 1970. Olivine-liquid equilibrium. *Contributions to Mineralogy and Petrology* 29: 275-289.

VULPIANI G., RIPEPE M., VALADE S., 2016. Mass discharge rate retrieval combining weather radar and thermal camera observations. *Journal of Geophysical Research: Solid Earth* 121: 5679-5695.

(ms. pres. 19 aprile 2018; ult. bozze 29 ottobre 2018)

Edizioni ETS
Palazzo Roncioni - Lungarno Mediceo, 16, I-56127 Pisa
info@edizioniets.com - www.edizioniets.com
Finito di stampare nel mese di febbraio 2019